

Supporting Information

In Silico Identification of JMJD3 Demethylase Inhibitors

C. Esposito, L. Wiedmer, and A. Caflisch*

Department of Biochemistry, University of Zurich, Winterthurerstrasse 190, CH-8057 Zurich,
Switzerland

*Corresponding author: caflisch@bioc.uzh.ch

TABLE OF CONTENTS

3	Table S1. Interaction energy values between known inhibitors and each of the investigated QM probes
4	Table S2. Results of single-dose measurements by the AlphaScreen assay at Reaction Biology Corporation
5	Table S3. Data collection and refinement of holo structures of UTX.
5	Table S4. Tanimoto similarity indices between compounds 10-13 and two aggregators
6	Figure S1. 5C8HQ pharmacophore features used for library and pose generation during the second virtual screening
6	Figure S2. QM probes used for the first and second virtual screening
7	Figure S3. Interaction energy distributions of compounds relative to the first campaign
8	Figure S4. Interaction energy distributions of compounds relative to the second campaign
9	Figure S5. Sequence conservation mapping of most KDM demethylases relative to JMJD3 and sequence alignment of the methylation sites in the N termini of histones H3 and H4
10	Figure S6. Evaluation of the predictive ability of the scoring function
11	Figure S7. Molecules selected from the first virtual screening campaign and inactive by Alphascreen assay
12	Figure S8. Molecules selected from the second virtual screening campaign and inactive by Alphascreen assay
13	Figure S9. Alphascreen dose-response experiments for compounds 1-4 and 7
14	Figure S10. Derivatives of hit 1 used for SAR studies
15	Figure S11. Alphascreen dose-response experiments for compounds 8-14
16	Figure S12. Electron density maps of GSK-J1 and 5C8HQ in complex with UTX
17	Figure S13. Metal-coordination rearrangement upon binding of different ligands
18	Figure S14. The purity of compound 8 was investigated by ¹ H NMR and HPLC-UV
19	Figure S15. Possible tautomeric and protonation equilibria of compounds 8 and 9
20	Figure S16. The chemical stability of compound 8 was investigated by HPLC-MS
21	Supporting References

Table S1. Interaction energy (*IE*) values in kcal/mol between known inhibitors and each of the investigated QM probes. The *IE* values were calculated by MOPAC at the semi-empirical PM7 level. QM probes were extracted from the crystallographic structures that were used for docking. In particular, during the first *in silico* campaign, QM probes were extracted from the JMJD3/5C8HQ complex (PDB 2XXZ) for the scoring of derivatives of scaffold **A** and from the JMJD3/GSK-J1 complex (4ASK) for derivatives of scaffolds **B-D** (see METHODS in the main text). Reference compounds GSK-J1 and 5C8HQ were docked into their respective crystal structures 4ASK and 2XXZ according to the pose generation procedure used for the first campaign. For the second *in silico* screening, QM probes were extracted only from 2XXZ (see also Figure S2). Accordingly, both reference compounds were docked into 2XXZ following the pose generation procedure of the second campaign. Probes atoms that were kept flexible during the minimization are shown in boldface type. The side chains of Asn and Gln were modelled by acetamide when exposed to the solvent or by hydrofluoric acid otherwise. In the particular case of Asn1393, both the backbone and sidechain NH groups were modelled by hydrofluoric acid. Asn1393 is located at the entrance of the binding site and in close proximity to GSK-J1 (PDB code: 4ASK). The closest distances between GSK-J1 heavy atoms and the backbone and sidechain nitrogen atoms of Asn1393 are 3.96 and 3.55 Å, respectively. Therefore, Asn1393 probes were selected in order to discard derivatives of scaffolds **C-D** having substituents giving unfavourable interactions with Asn1393. The different interaction energy values observed for the first and second campaign for the interactions between 5C8HQ and the probes representing Tyr1379, Lys1381 and Thr1387 are a consequence of the different procedures used for the pose generation. This difference is significant in the case of the interaction between the carboxyl group of 5C8HQ and the Lys1381 side chain (-46.7 kcal/mol in 4ASK and -120.1 kcal/mol in 2XXZ) because of the strong dependence of ionic interactions on the interionic distance.

FIRST CAMPAIGN				
Residue	QM Probe		GSK-J1 in 4ASK	5C8HQ in 2XXZ
Asn1331	CH₃CONH₂	Acetamide	-9.2	-2.0
Gln1377	CH₃CONH₂	Acetamide	-3.6	-0.8
Tyr1379	CH₃OH	Methanol	-1.0	-3.6
Lys1381	CH₃NH₃⁺	Methyl Ammonium	-121.0	-46.7
Thr1387	CH₃OH	Methanol	-10.9	-6.8
Asn1393bb	HF	Hydrofluoric acid	-1.0	-0.1
Asn1393	HF	Hydrofluoric acid	0.1	0.1
Ser1398	CH₃OH	Methanol	0.6	-0.9
Asn1400	HF	Hydrofluoric acid	-17.8	-8.0
SECOND CAMPAIGN				
Residue	QM Probe		GSK-J1 in 2XXZ	5C8HQ in 2XXZ
Gln1377	CH₃CONH₂	Acetamide	-0.3	-0.5
Tyr1379	CH₃OH	Methanol	-7.8	-4.9
Lys1381	CH₃NH₃⁺	Methyl Ammonium	-121.3	-120.1
Thr1387	CH₃OH	Methanol	-13.1	-5.3
Gly1389bb	H ₂ O	Water	-0.9	-0.6
Gly1435bb	H ₂ O	Water	0.3	0.5

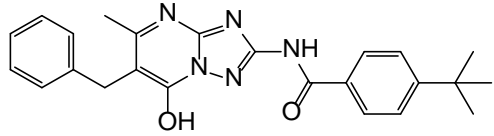
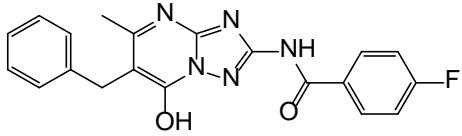
Table S2. Results of single-dose measurements by the AlphaScreen assay at Reaction Biology Corporation. Data 1 and 2 refer to duplicate measurements. Compounds **1-6** and **S1-S6** were tested directly by dose-response measurements and here we report the value at the highest concentration of 200 μ M. Molecules with solubility issues are highlighted in red.

Compound ID	%Enzyme activity relative to DMSO			% DMSO in reaction
	Test conc (μ M)	JMJD3		
		Data 1	Data 2	
1	200	-19		0.4
2	200	-26		0.4
3	200	13		0.4
4	200	6		0.4
5	200	67		0.4
6	200	98		0.4
7	500	0	0	1
8	100	15	14	1
9	250	1	1	1
10	500	2	3	2
11	500	7	14	5
12	500	-4	-6	1
13	500	1	4	1
14	500	4	3	1
S1	200	95		1
S2	200	71		1
S3	200	76		1
S4	200	100		1
S5	200	98		1
S6	200	107		1
S7	500	90	87	1
S8	500	27	21	1
S9	500	97	94	1
S10	500	58	56	1
S11	500	38	42	1
S12	500	83	90	1
S13	500	95	93	1
S14	500	62	69	1
S15	500	74	78	1
S16	500	77	80	1
S17	500	73	88	1
S18	500	73	75	1
S19	500	73	76	1

Table S3. Data collection and refinement of holo structures of UTX.

PDB code	6G8F	6FUL	6FUK
Inhibitor	GSK-J1	Compound 8	5C8HQ
Metal	Mn ²⁺	Mn ²⁺	Mn ²⁺
Data collection			
Space group	P2 ₁ 2 ₁ 2 ₁	P2 ₁ 2 ₁ 2 ₁	P2 ₁ 2 ₁ 2 ₁
Unit Cell Parameters			
a, b, c (Å)	80.78, 82.34, 92.40	79.18, 82.80, 93.16	80.42, 83.26, 92.90
α, β, γ (°)	90.00, 90.00, 90.00	90.00, 90.00, 90.00	90.00, 90.00, 90.00
Resolution (Å)	48.92 - 2.04	48.76 - 1.65	46.45-2.00
Unique observations*	72632 (11283)	138199 (22076)	42377 (6776)
Completeness (%)	96.1 (92.3)	96.9 (95.8)	98.3 (98.4)
Redundancy*	2.0 (1.9)	2.0 (1.9)	3.7 (3.7)
Rmeas (%)	4.9 (66.6)	7.2 (67.3)	5.8 (79.1)
I/σ*	11.1 (1.4)	8.0 (1.4)	12.6 (1.7)
Refinement			
Rwork / Rfree (%)	19.1 / 23.5	17.6 / 20.8	18.6 / 22.8
Ramachandran			
Favored (%)	97.0	97.2	97.2
Disallowed (%)	0.0	0.0	0.0
R.m.s. deviations			
Bond lengths (Å)	0.009	0.007	0.009
Bond Angles (°)	0.775	0.803	0.806

Table S4. Tanimoto similarity indices between compounds **10-13** and the two aggregators that have been identified by the Aggregators Advisor Web server.¹ Similarity values were calculated using the Similarity Workbench of ChemMine tools.²

Compound ID		
10	0.34	0.39
11	0.28	0.32
12	0.31	0.35
13	0.36	0.50

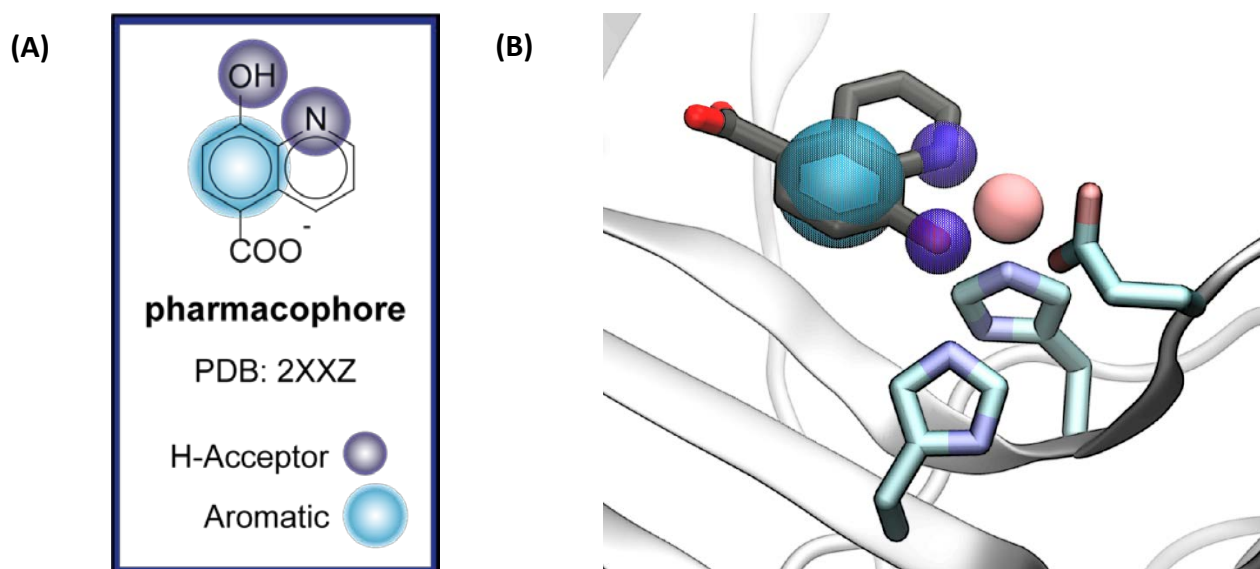


Figure S1. 5C8HQ pharmacophore features used for library and pose generation during the second virtual screening are shown in (A) 2D and (B) 3D. Hydrogen bond acceptors are shown in blue, while the aromatic sphere is shown in cyan.

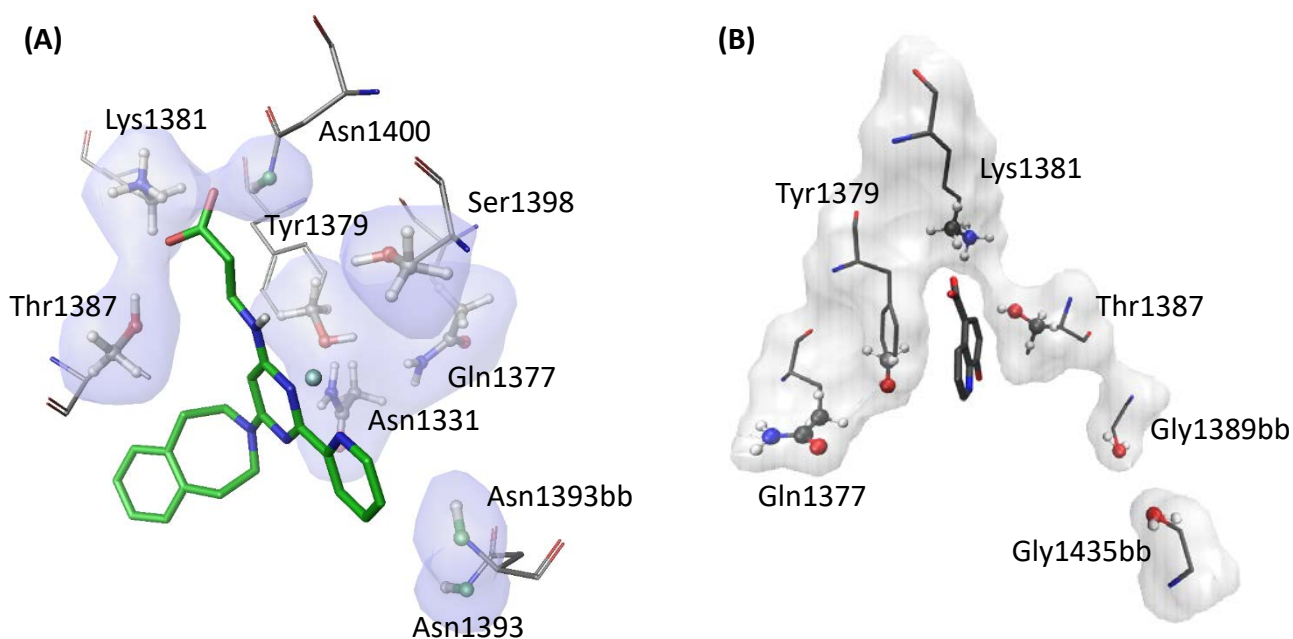


Figure S2. QM probes used for the (A) first and (B) second virtual screening campaign originate from the structure of the JMJD3 complex with GSK-J1 (carbon atoms in green) and 5C8HQ (carbon atoms in grey), respectively. The QM probes on the backbone are labelled as “bb”.

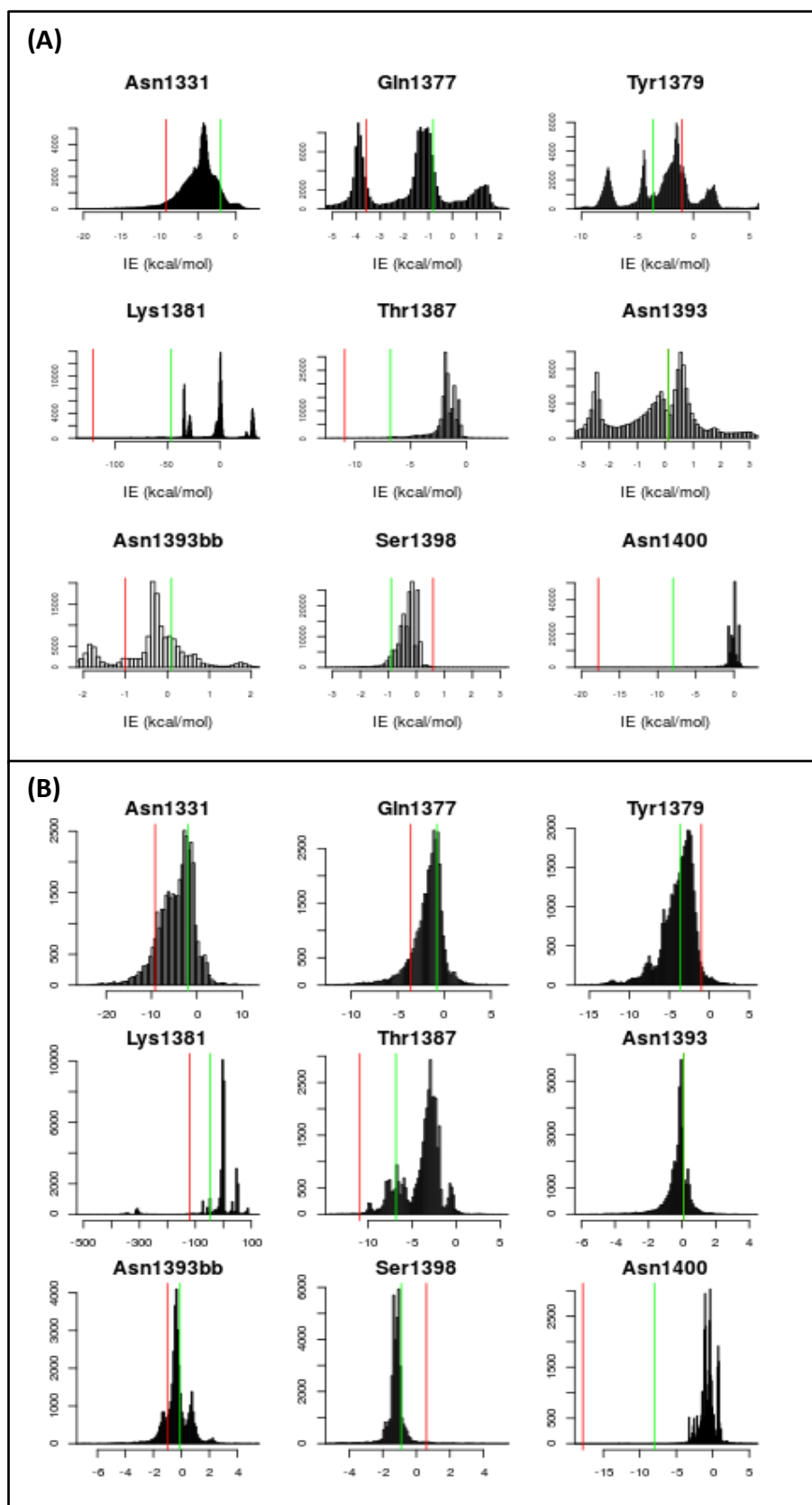


Figure S3. Interaction energy (*IE*) distributions of compounds relative to the first campaign for each of the investigated QM probes. Red and green lines show the interaction energy values of GSK-J1 (PDB code: 4ASK) and 5C8HQ (PDB code: 2XXZ), respectively. (A) Derivatives of scaffolds **B-D**, docked into 4ASK. (B) Derivatives of scaffold **A**, docked into 2XXZ.

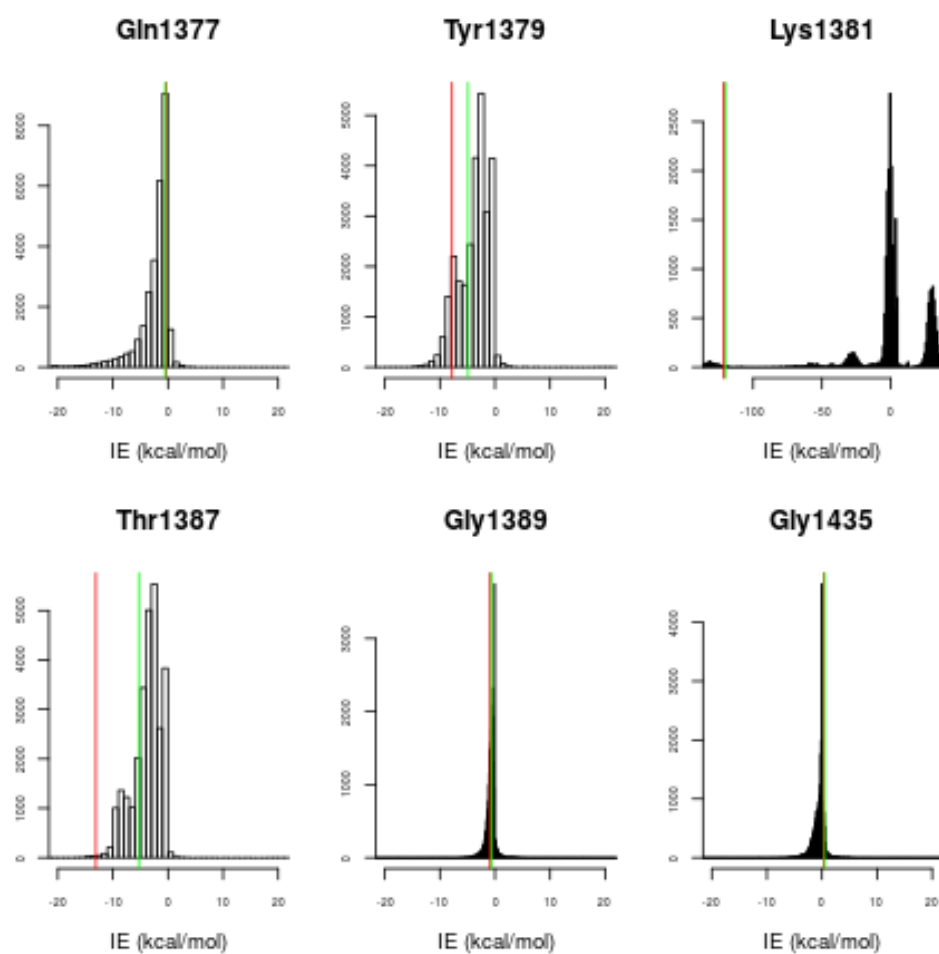


Figure S4. Same as figure S3 for the second campaign. Red and green lines show the *IE* values of GSK-J1 and 5C8HQ, which were both docked into 2XXZ crystallographic structure. All *IE* were calculated with respect to QM probes derived from 2XXZ.

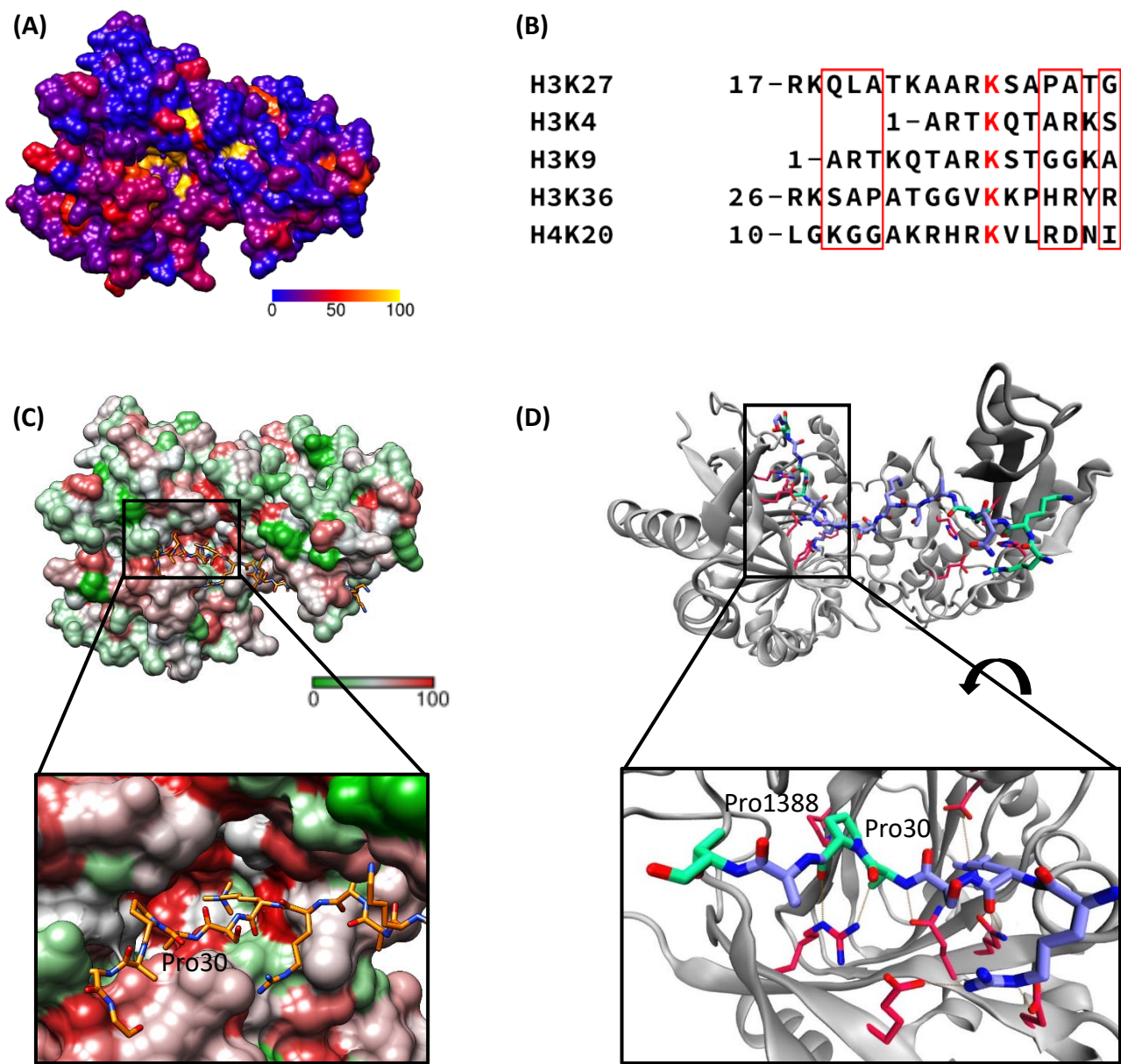
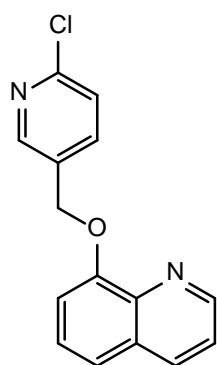
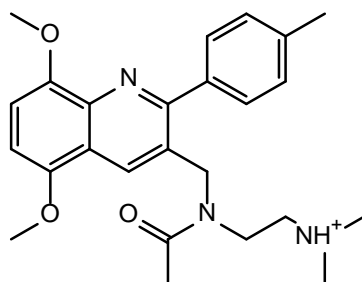


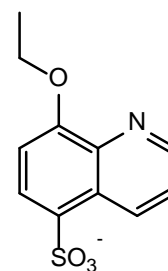
Figure S5. (A) Family sequence conservation mapping of most KDM demethylases relative to JMJD3 (also called KDM6B). Residue conservation percentage is coloured from yellow (invariant) to blue (variable) and was measured as follows: first, the aligned sequences of Human KDM2 (A, B), KDM4 (A, B, C, D, E), KDM5 (A, B, C, D, JARID2) and KDM6 (A, B, C) were downloaded from the web server Uniprot; second, conservation frequency was calculated relative to the JMJD3 sequence as the ratio between the occurrence of the JMJD3 residue and the number of proteins. (B) Sequence alignment of N termini H3 and H4 segments based on the position of the methylated lysine, each recognized specifically by a different demethylase. Red squares indicate unique residues around H3K27.^{3,4} (C) Family sequence similarity mapping. The similarity percentage was calculated as in panel (A) but splitting the amino acids in five groups: neutral apolar (Ala, Gly, Ile, Leu, Met, Pro, Val), neutral polar (Asn, Cys, Gln, Ser, Thr), positively charged (Arg, Lys), negatively charged (Asp, Glu) and aromatic (His, Phe, Trp, Tyr). The zoom shows that Pro30 of H3 is located in a poorly conserved subpocket. (D) H3K27 binds to both the catalytic and the zinc finger domain of JMJD3. The zoom shows that Pro30 of the H3 interacts with Pro1388 of JMJD3.



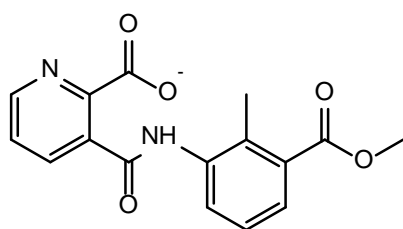
S1



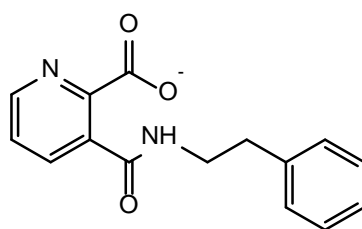
S2



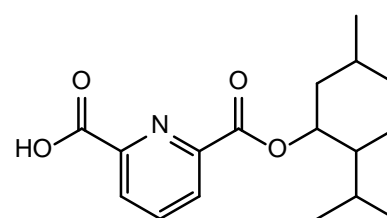
S3



S4



S5



S6

Figure S6. Molecules selected from the first virtual screening campaign and inactive by Alphascreen assay. Compounds **S1-S3** are derivatives of scaffold **A** while compounds **S4-S6** are derivatives of scaffold **B** (Figure 1).

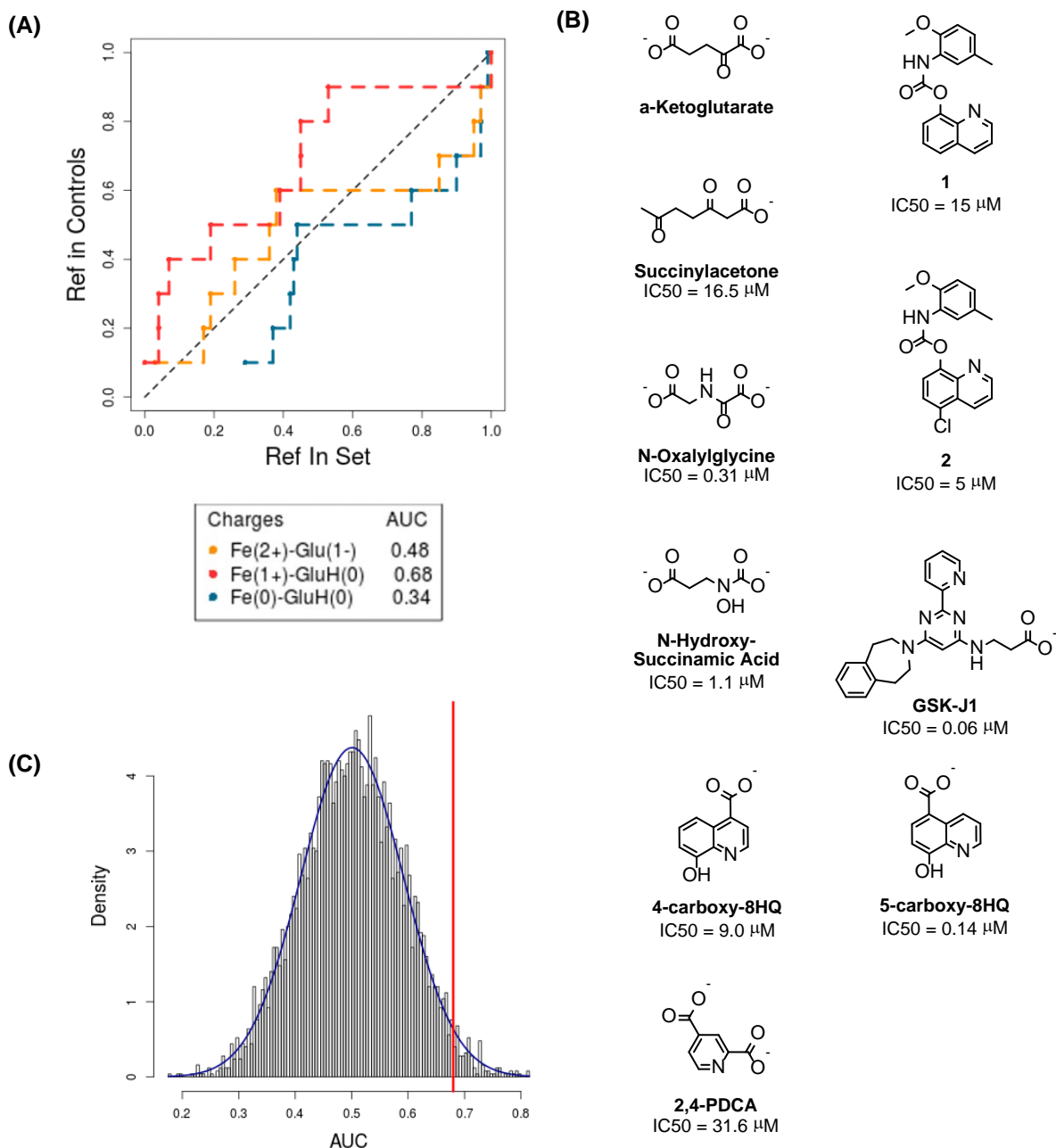


Figure S7. Evaluation of the predictive ability of the scoring function. (A) ROC curves show the enrichment of true positives. The database of decoys contains the subset of 18278 conformers of 6091 compounds from the focused library of novel scaffolds (orange flowchart in Figure 1), which were minimized and scored by CHARMM. The CHARMM total binding energy was calculated using three different Fe-Glu1392 charge distributions (see legend): Fe(2+)-Glu1392(1-), Fe(1+)-GluH(0), and Fe(0)-GluH(0). The highest value of AUC = 0.68 was obtained for the total binding energy calculated according to the charge redistribution Fe(1+)-GluH(0). The dotted black line represents the results expected from random selection of ligands. (B) Known JMJD3 inhibitors⁵⁻⁹ and compounds **1-2** identified in this work, which were used as true positives. (C) To assess the significance of the AUC, we randomly sampled the positions of the 10 true actives among the 18278 decoys. The experiment was repeated 5000 times and a distribution of AUC was built. The histogram of AUC is shown in black, while the normal distribution fit is shown in blue; the red line illustrates the AUC obtained for the best performing binding energy function (Fe(1+)-GluH(0)). Under the null hypothesis that the information provided by the true actives does not allow to distinguish between true actives and false positives, the probability of having an AUC higher than 0.68 is $\leq 2.5\%$. In other words, based on the one-tailed t-test, we can reject the null hypothesis with a probability $> 97.5\%$.

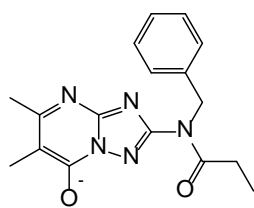
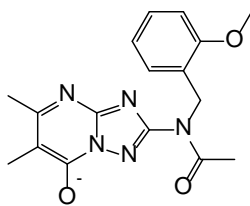
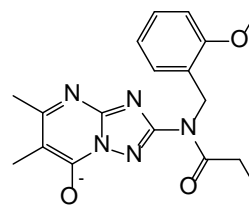
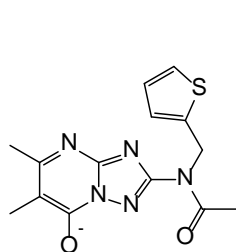
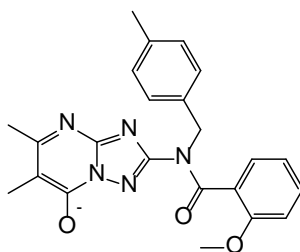
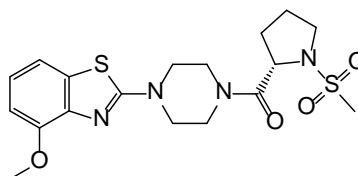
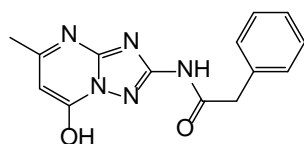
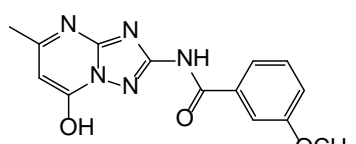
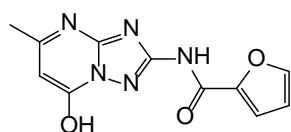
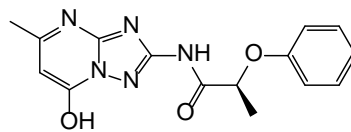
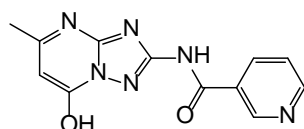
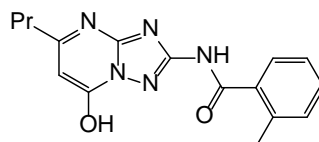
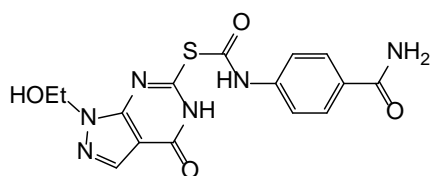
**S7****S8****S9****S10****S11****S12****S13****S14****S15****S16****S17****S18****S19**

Figure S8. Molecules selected from the second virtual screening campaign and inactive by Alphascreen assay. Compounds **S7-S12** are derivatives of scaffold **H** (Figure 1). Compounds **S13-S19** were selected from the ChemDiv library based on pharmacophore similarity to 5C8HQ (purple flowchart in Figure 1).

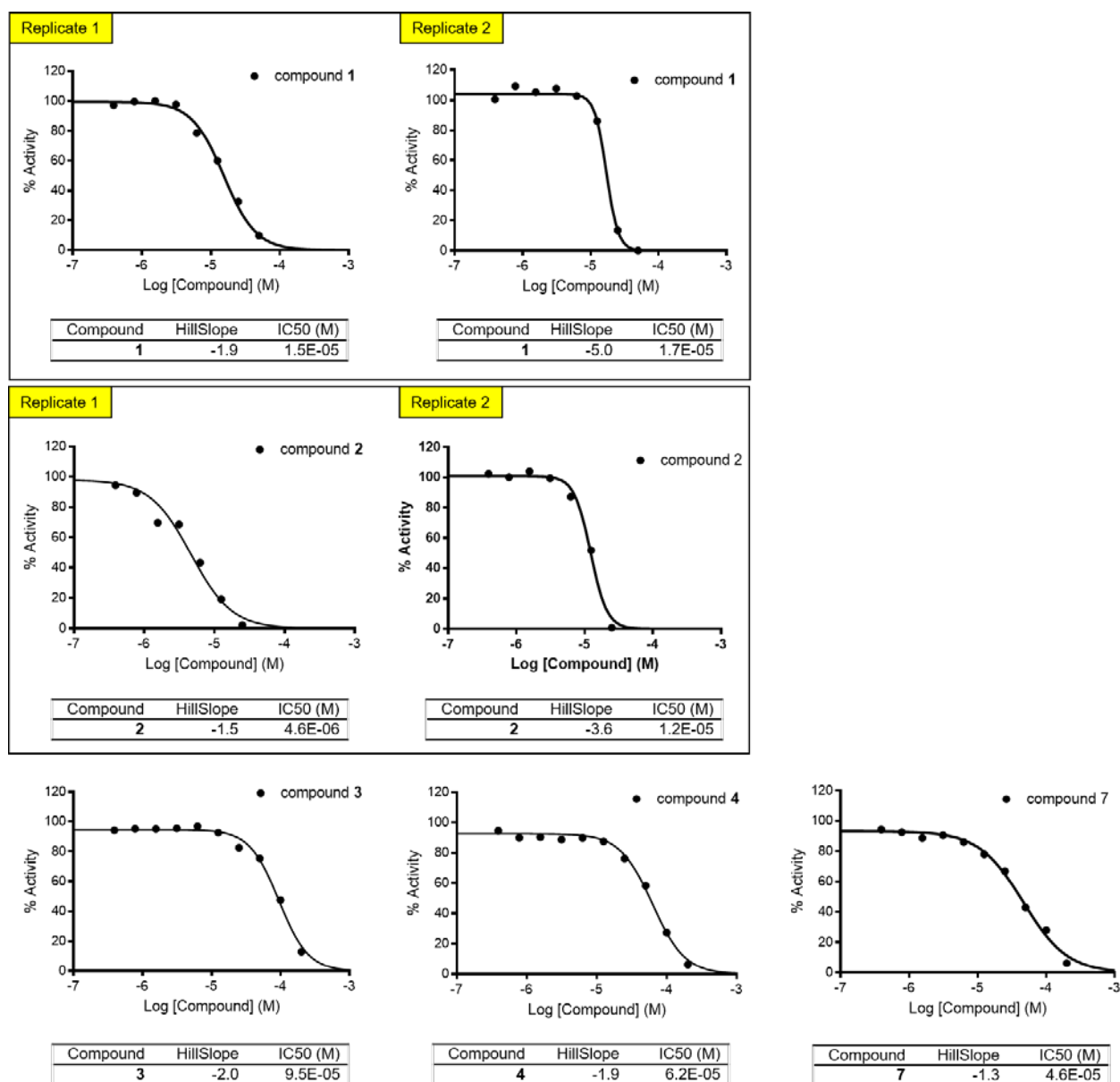


Figure S9. In vitro validation of first screening campaign. Alphascreen dose-response experiments for compounds **1-4** and **7** were carried out at Reaction Biology Inc. Replicates were measured only for compound **1** (the original hit from tethered docking) and its derivative **2** (the most potent compound of the hit expansion). Note that compounds **5** and **6** were selected as negative controls and, as predicted, they do not show binding at a concentration of 200 μ M.

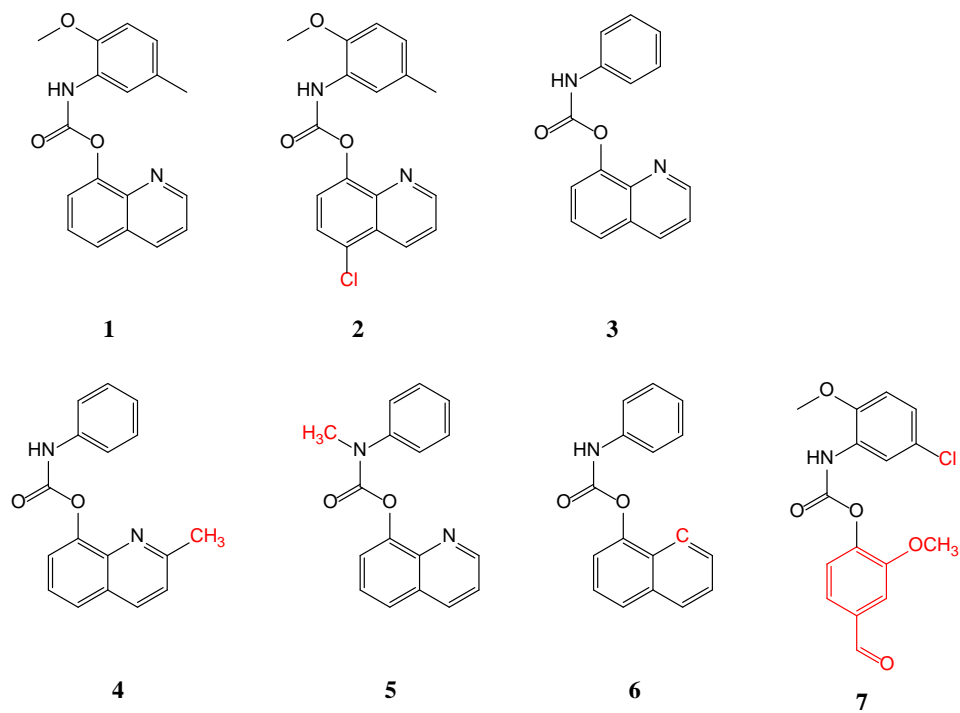
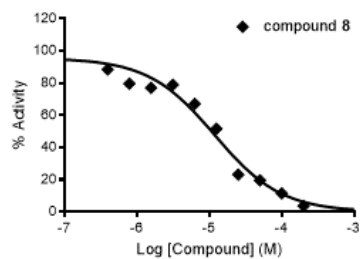
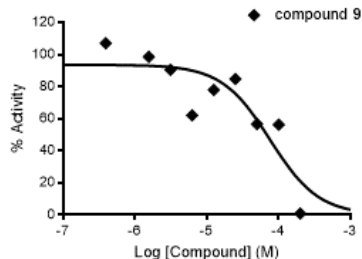


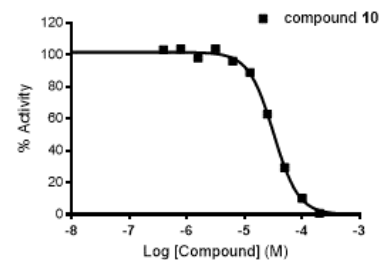
Figure S10. Derivatives of hit **1** used for SAR studies. Differences are highlighted in red.



Compound	HillSlope	IC50 (M)
8	-0.94	1.2E-05

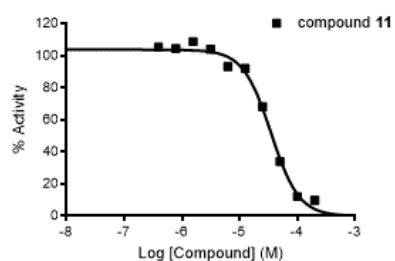


Compound	HillSlope	IC50 (M)
9	-1.3	7.6E-05



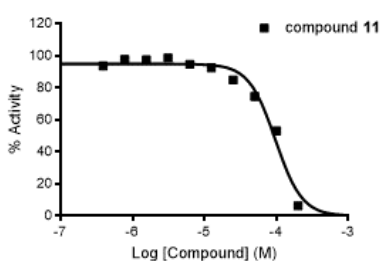
Compound	HillSlope	IC50 (M)
10	-2.0	3.2E-05

Replicate 1

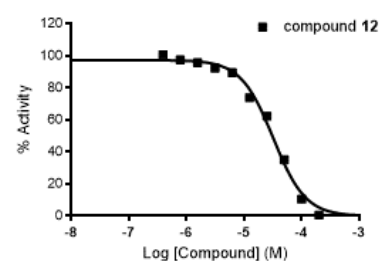


Compound	HillSlope	IC50 (M)
11	-1.8	3.5E-05

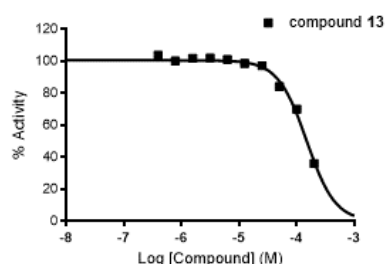
Replicate 2



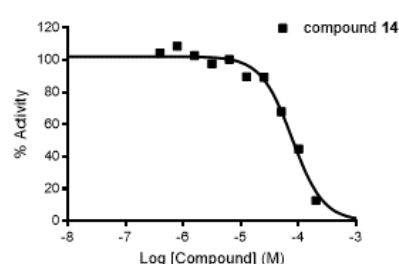
Compound	HillSlope	IC50 (M)
11	-2.4	9.7E-05



Compound	HillSlope	IC50 (M)
12	-1.6	3.2E-05



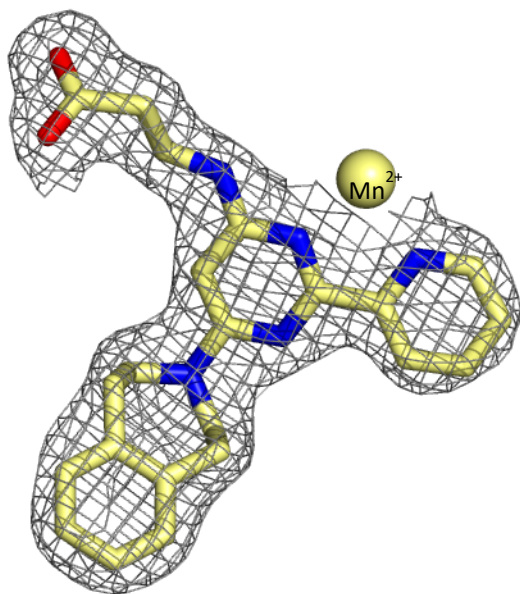
Compound	HillSlope	IC50 (M)
13	-1.8	1.5E-04



Compound	HillSlope	IC50 (M)
14	-1.6	7.7E-05

Figure S11. In vitro validation of second screening campaign. Alphascreen dose-response experiments for compounds 8-14 were carried out at Reaction Biology Inc. Replicates were measured only for compound 11.

(A)



(B)

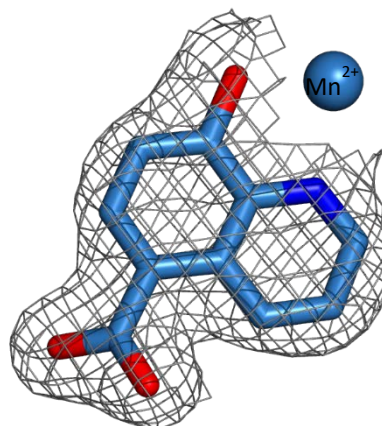


Figure S12. Electron density maps of known inhibitors, (A) GSK-J1 (PDB code: 6G8F) and (B) 5C8HQ (PDB code: 6FUK) in complex with UTX. The 2Fo-Fc electron density map is shown by a mesh contoured at 1 σ .

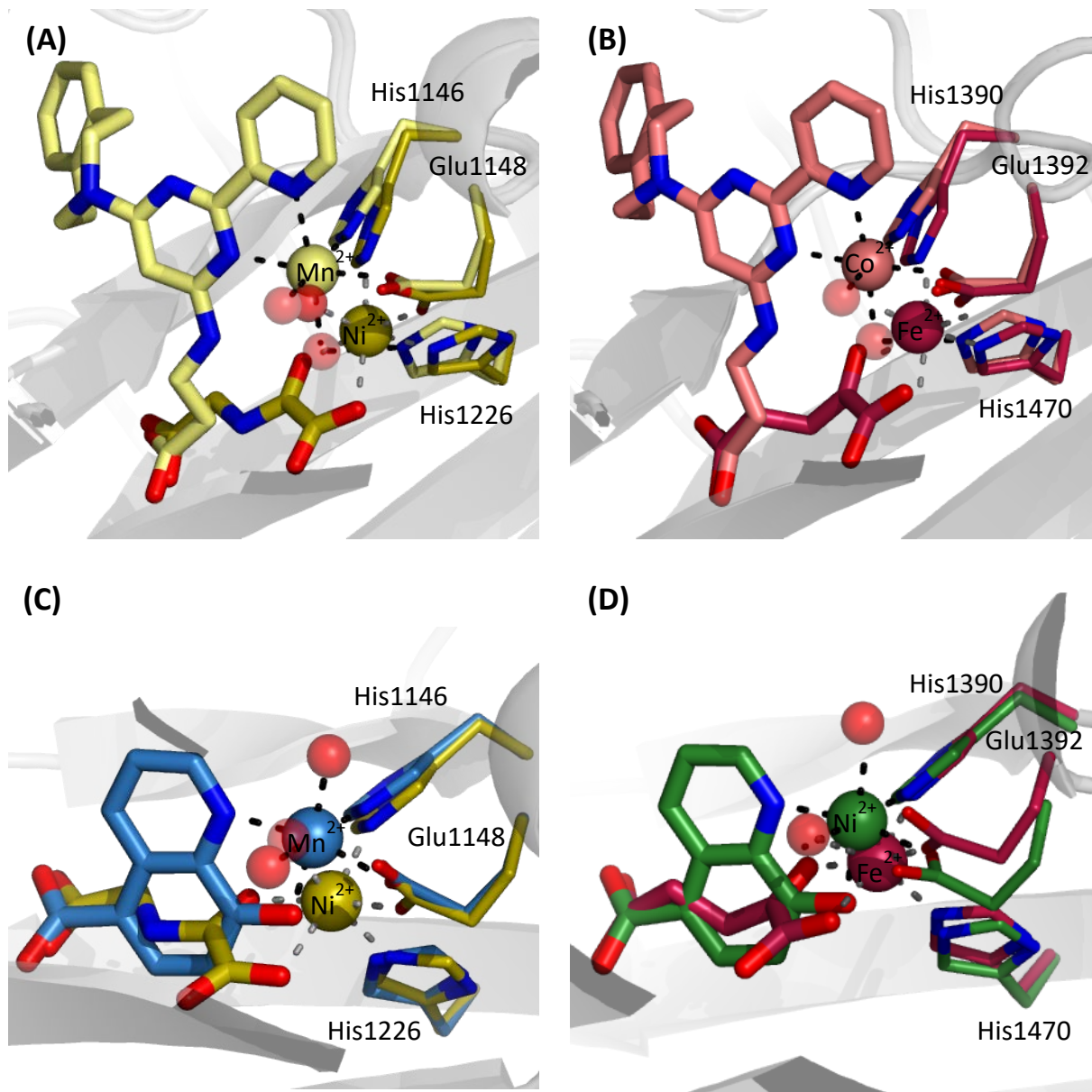


Figure S13. Metal-coordination rearrangement upon binding of different ligands. (A) GSK-J1 vs. NOG in UTX (PDB codes: 6G8F and 3AVS). (B) GSK-J1 vs. OGA in JMJD3 (PDB codes: 4ASK and 2XUE). (C) 5C8HQ vs. NOG in UTX (PDB codes: 6FUK and 3AVS). (D) 5C8HQ vs. OGA in JMJD3 (PDB codes: 2XXZ and 2XUE). Compounds and residues are coloured consistently with the main text.

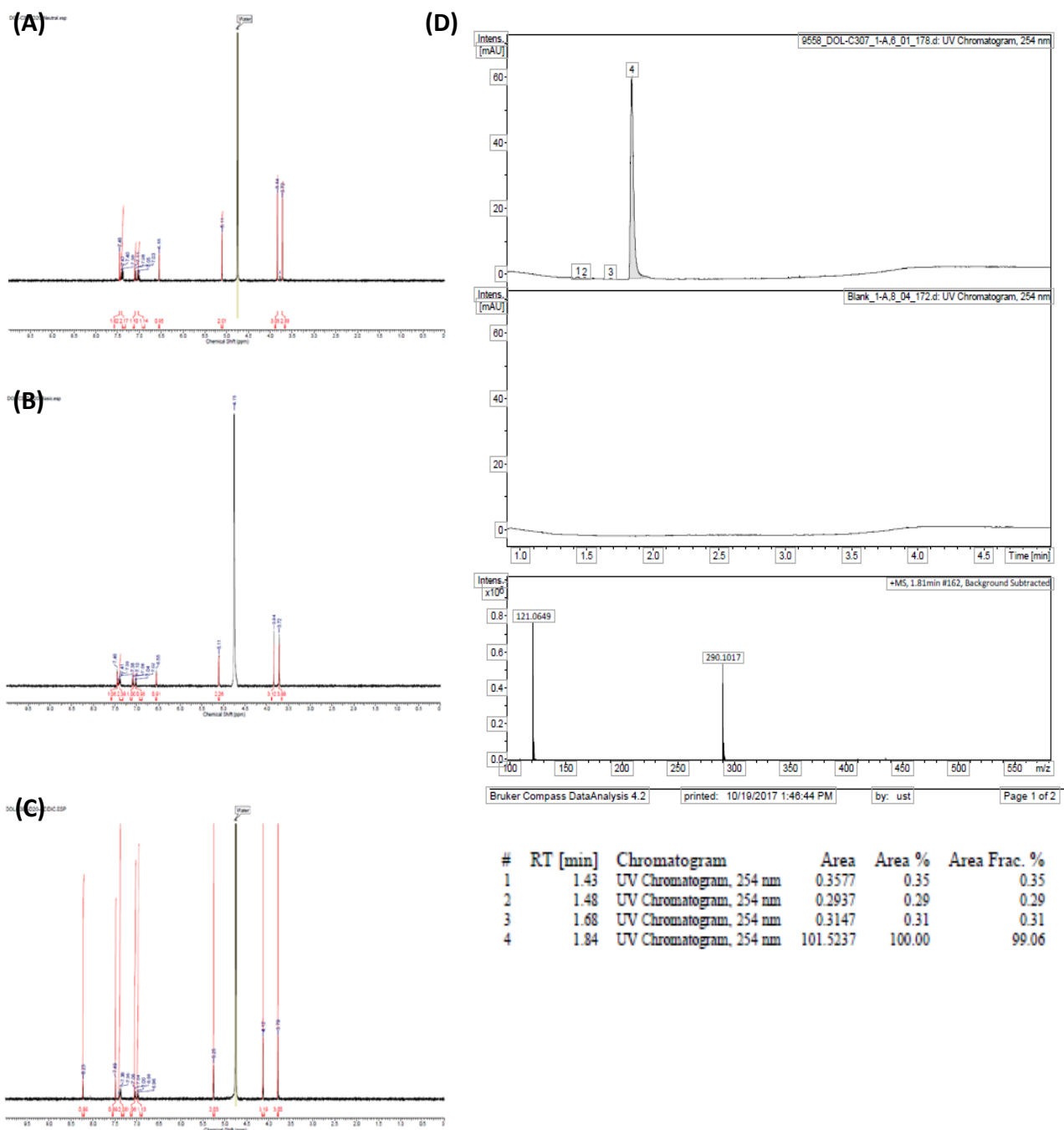


Figure S14. The purity of compound **8** was investigated by ^1H NMR in (A) neutral, (B) basic, and (C) acidic conditions, and (D) by HPLC-UV. The three samples of compound **8** for ^1H NMR measurements were prepared, as follows. Neutral conditions, pH \sim 7: compound **8** (0.5 mg) was dissolved in 500 μl of D_2O . Acid conditions, pH \sim 1: compound **8** (0.5 mg) was dissolved in 400 μl of D_2O and 100 μl of a 0.1 M HCl solution (distilled H_2O) were added. Basic conditions, pH \sim 14 (pH paper): compound **8** (0.5 mg) was dissolved in 400 μl of D_2O and 100 μl of a 0.1 M NaOH solution (distilled H_2O) were added. The solutions were transferred into one NMR tube and ^1H -NMR of the samples were recorded on a AV2 400 MHz Bruker spectrometer. Spectra were calibrated to the residual ^1H signal of the solvent (For D_2O : 4.75 ppm). The purity of compound **8** (100 $\mu\text{g}/\text{mL}$ in MeOH/DMSO 9:1) was determined by HPLC on a Acquity UPLC (Waters, Milford, MA) top spectrometer using an Acquity CSH C18 column (1.7 μm , 2.1×100 mm, Waters) and a mixture of water + 0.1 % acetic acid and acetonitrile + 0.1 % formic acid as solvent. High resolution electrospray ionization mass spectrometry was performed on a Bruker maXis Q-ToF mass spectrometer (Bruker Daltonics, Bremen, Germany).

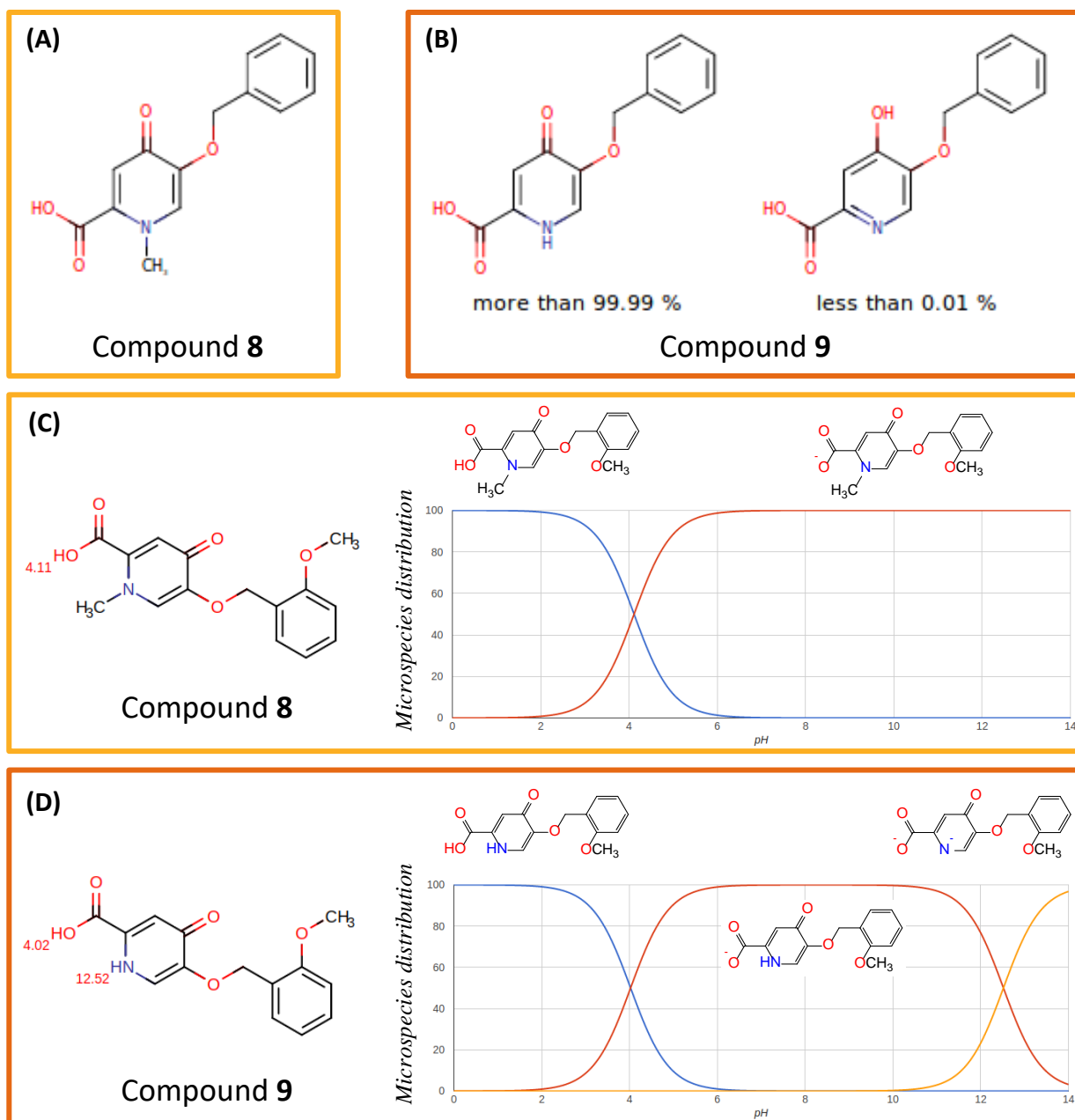


Figure S15. Possible tautomeric and protonation equilibria of compounds **8** (light orange) and **9** (dark orange). (A-B) Tautomeric forms were predicted using the Tautomer Generator Plugin of ChemAxon¹⁰, (C-D) while protonation states in the pH range 0-14 were estimated using the Chemicalize Web server.¹¹

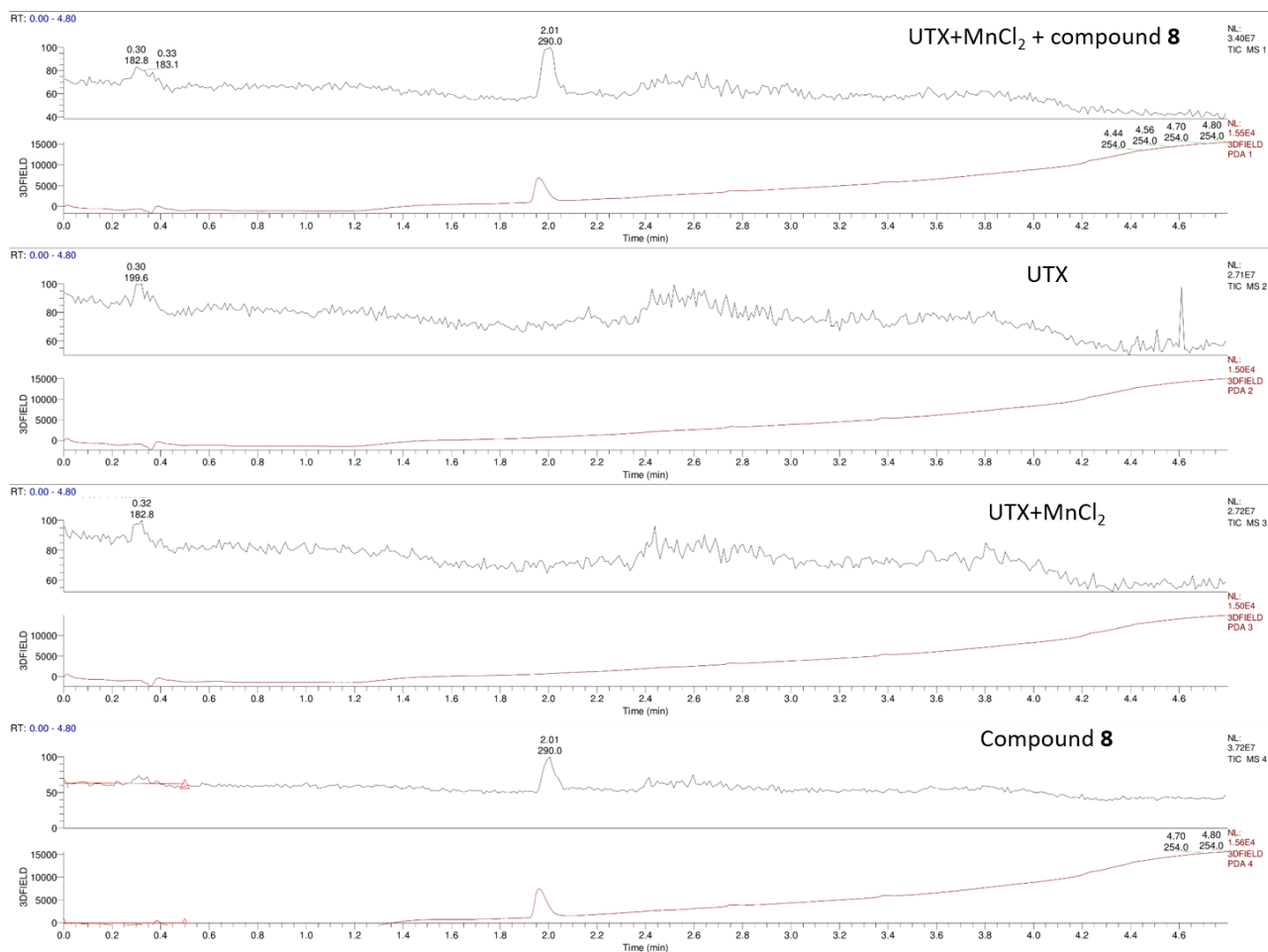


Figure S16. The chemical stability of compound **8** in the crystallization conditions was investigated by LC-UV/MS. The following mixture was incubated overnight at 4 °C: 10 mM compound **8**, 1 μ M UTX, 1mM MnCl₂, 100mM Tris-HCl (pH 8.0), 150 mM NaCl. Control experiments were performed in which UTX, MnCl₂ or compound **8** were separately or together left out of the reaction mixture. Low molecular weight solutes were subsequently separated from the protein solution by using 10K cutoff filter (Amicon). LC/UV/MS analysis provided information on the extracted solutes. For each measurement, the MS trace is illustrated in the upper panel, while the UV trace at 254 nm is shown in the lower panel.

SUPPORTING REFERENCES

1. Irwin, J. J.; Duan, D.; Torosyan, H.; Doak, A. K.; Ziebart, K. T.; Sterling, T.; Tumanian, G.; Shoichet, B. K., An Aggregation Advisor for Ligand Discovery. *Journal of medicinal chemistry* **2015**, *58*, 7076-7087.
2. Backman, T. W.; Cao, Y.; Girke, T., ChemMine Tools: an Online Service for Analyzing and Clustering Small Molecules. *Nucleic acids research* **2011**, *39*, W486-W491.
3. Martin, C.; Zhang, Y., The Diverse Functions of Histone Lysine Methylation. *Nature reviews Molecular cell biology* **2005**, *6*, 838-849.
4. Pedersen, M. T.; Helin, K., Histone Demethylases in Development and Disease. *Trends in cell biology* **2010**, *20*, 662-671.
5. Rotili, D.; Tomassi, S.; Conte, M.; Benedetti, R.; Tortorici, M.; Ciossani, G.; Valente, S.; Marrocco, B.; Labella, D.; Novellino, E., Pan-Histone Demethylase Inhibitors Simultaneously Targeting Jumonji C and Lysine-Specific Demethylases Display High Anticancer Activities. *Journal of medicinal chemistry* **2013**, *57*, 42-55.
6. Hopkinson, R. J.; Tumber, A.; Yapp, C.; Chowdhury, R.; Aik, W.; Che, K. H.; Li, X. S.; Kristensen, J. B.; King, O. N.; Chan, M. C., 5-Carboxy-8-Hydroxyquinoline is a Broad Spectrum 2-Oxoglutarate Oxygenase Inhibitor which Causes Iron Translocation. *Chemical science* **2013**, *4*, 3110-3117.
7. Kruidenier, L.; Chung, C.-w.; Cheng, Z.; Liddle, J.; Che, K.; Joberty, G.; Bantscheff, M.; Bountra, C.; Bridges, A.; Diallo, H., A Selective Jumonji H3K27 Demethylase Inhibitor Modulates the Proinflammatory Macrophage Response. *Nature* **2012**, *488*, 404.
8. Rose, N. R.; Woon, E. C.; Tumber, A.; Walport, L. J.; Chowdhury, R.; Li, X. S.; King, O. N.; Lejeune, C.; Ng, S. S.; Krojer, T., Plant Growth Regulator Daminozide is a Selective Inhibitor of Human KDM2/7 Histone Demethylases. *Journal of medicinal chemistry* **2012**, *55*, 6639-6643.
9. England, K. S.; Tumber, A.; Krojer, T.; Scozzafava, G.; Ng, S. S.; Daniel, M.; Szykowska, A.; Che, K.; von Delft, F.; Burgess-Brown, N. A., Optimisation of a Triazolopyridine Based Histone Demethylase Inhibitor Yields a Potent and Selective KDM2A (FBXL11) Inhibitor. *MedChemComm* **2014**, *5*, 1879-1886.
10. Calculator Plugins were Used for Structure Property Prediction and Calculation. Marvin 15.1.5.0, ChemAxon (www.chemaxon.com) **2015**.
11. Swain, M., In; ACS Publications: 2012.